





Construction Process Simulation of Building Decoration based on BIM and Computer-Aided Technology

Yugang Dong^{1*}, Yingqun Zhang² and Fangfang Sang³

^{1,2,3}Weifang Engineering Vocational College, Qingzhou 262500, China

¹YugangDong@aliyun.com, ²zhanglange2010@sina.com,

³Sangff2010@sina.com

Corresponding author: Yugang Dong, YugangDong@aliyun.com

Abstract. In order to improve the efficiency of architectural decoration design and construction, this paper proposes an image stitching algorithm based on feature points and a camouflage stitching algorithm based on transition columns. Moreover, this paper uses texture synthesis technology to expand the border of the pattern to be spliced, and generates an expanded pattern with natural texture transition. Taking into account the characteristics of digital camouflage, this paper selects two-step texture mapping as the main technical means in 3D digital camouflage design, and uses a model based on similarity features such as structure, texture, color, and second-order statistical moments as the core content of the evaluation of camouflage effect. In addition, this paper uses the above algorithm to improve the computer-aided technology, and combines BIM technology and computer-aided technology to jointly simulate the building decoration construction process. Finally, this paper designs experiments to verify the effects of the algorithms and simulation methods proposed in this paper. The research results show that the model constructed in this paper has certain practical effects.

Keywords: BIM; computer-aided technology; architectural decoration; construction simulation

DOI: <https://doi.org/10.14733/cadaps.2023.S15.294-308>

1 INTRODUCTION

Simulation technology is a new comprehensive technology that conducts experimental research on real or virtual systems through simulation models. It is based on similar principles, information technology, graphics and image technology, automatic control technology and related professional technologies in its application fields, and uses computers and various physical effect devices as simulation tools.

Under the architectural requirements of functionalized architectural decoration, complex structural modeling, and expanded scale, traditional construction techniques and methods are

Computer-Aided Design & Applications, 20(S15), 2023, 294-308

© 2023 CAD Solutions, LLC, <http://www.cad-journal.net>

difficult to meet and achieve [13]. As a pillar industry of our country, architecture contains a large amount of engineering information throughout its life cycle from design, construction, and operation, and requires strong technology to support it. The complete set of technologies with BIM research and application as the core is an important means to promote the technological upgrading and transformation of the construction industry. At present, it has received widespread attention in the industry, and has achieved remarkable results, and has promoted the transformation of the construction industry from a traditional model to a multi-dimensional, refined, and informatized model [22].

In actual construction, the vertical deformation can be controlled by leveling or reserved length for construction. Different construction speeds and advanced construction layers of the core will affect the vertical deformation and the vertical deformation difference of the structure. When the assumptions of these two factors in the structural analysis and calculation at the design stage are different from the actual construction, the actual vertical deformation of the structure may be far from the calculated result. At this time, it may be necessary to re-calculate and analyze to obtain the new floor reserved elevation and vertical member blanking reserved length, or take new measures to control the adverse effects of vertical deformation on the building. The construction time of super high-rise buildings is long and there is a risk of shutdown. Scholars at home and abroad have rarely studied the impact of shutdown on the vertical deformation of structures. However, the actual analysis needs to consider the influencing factor of work stoppage [18]. Therefore, it is necessary to study the influence of advanced construction of core tube, construction speed and shutdown on the vertical deformation difference of super high-rise structure.

2 RELATED WORK

The literature [4] demonstrated and analyzed the application value of BIM at this stage. The literature [16] studied the benefits of IFC-based 4D model to team management and graphical processing. Aiming at the problem of low efficiency and waste of resources, the literature [12] elaborated on the necessity of informatization in the construction industry. The literature [23] analyzed the economic benefits brought by BIM virtual technology to relevant stakeholders and the future development trend of BIM. In view of the cumbersome and complicated data information processing of multiple participants, the literature [11] proposed the basic idea of applying BIM to the management of building information flow, and realized the Internet information technology of data sharing. Based on actual case experience, the literature [6] completed the free exchange of BIM technical data by establishing a data integration framework management system. The literature [7] introduced the method and process of IFC data transmission, and gave high affirmation and expectations for the future development of BIM. Based on the BIM concept and parametric design technology, literature [5] used the parametric software Rhinoceros to study the meshing theory and method of complex curved surfaces, the construction of curved curtain walls, and the generation logic. Moreover, it established a three-dimensional model of the free-form surface steel structure cover and performed software analysis and optimization of the structural plan, and proposed a whole process method for modeling and analysis of complex curved surfaces. Based on BIM-related theories and software, literature [2] studied the basic process of Tekla Structure to create airport BIM models for the complex working conditions and engineering difficulties of long-span special-shaped steel structure projects, which solved the problems of the installation accuracy of large-span arch truss, the construction and processing of the vault node, and the large foundation node. Based on the BIM three-dimensional modeling technology, the literature [17] developed the Civil 3D visualization software for the research topic of drawing and display of special-shaped steel structure models, which achieved the full-dimensional dynamic display effect of special-shaped steel components. The literature [4] applied BIM technology to the protection of industrial heritage buildings, proposed the

concept of "information index model", and completed a complete set of procedures for the collection, processing, modeling and later data management of industrial heritage information.

The literature [22] introduced the development status and existing problems of virtual construction technology abroad. The literature [21] expounded the concept of BIM virtual construction technology and its operation steps and simulates the 3D model visualization construction process, which shortens the project period, reduces the construction cost, and maximizes the benefits of all participants. Based on BIM-based virtual construction technology and construction monitoring analysis, the literature [19] effectively combined construction process visualization, construction mechanics simulation and on-site monitoring, which solves the construction problems of large and complex steel structures. Based on the BIM virtual construction technology, the literature [8] conducted simulations, comparative analysis and selected the optimal construction plan for two different construction plans of the Nanchang high-speed railway station. The literature [15] describes the project schedule based on the BIM model to calculate the duration of the construction process. The literature [10] understood BIM as a technical means for coordinating related professional work. The literature [1] used Revit to create a comprehensive model of architecture, structure and electromechanical projects, and uses Navisworks software to perform virtual construction simulation to achieve collision detection and analysis among various disciplines, and to ensure the safe construction of engineering projects. For actual engineering, the literature [20] used BIM for collision detection, established a comprehensive pipeline building information model, and used comprehensive collision software and visualization functions for pipeline collision detection, which can timely feedback the collision results to the construction personnel. The literature [14] analyzes the BIM solution to the spatial conflict of the temporary facility model. The literature [9] completed the collision inspection of electromechanical pipelines based on BIM visual modeling technology, and proposed the processing method of complex steel joints and the solution of collision results. The literature [3] conducted a theoretical analysis of the collision problem during construction, optimized the construction plan through construction simulation, and studied collision detection during automatic pipeline layout and how to avoid collisions.

3 COMPUTER-AIDED SIMULATION TECHNOLOGY

Image mosaic algorithms based on feature point matching usually directly use weighted fusion to complete the mosaic operation in the early days. The algorithm finds the most similar segmentation line by evaluating and calculating the difference in overlapping areas, so that the images on both sides of the segmentation line can be seamlessly stitched at the segmentation line. This segmentation line is the best suture line we are looking for.

The calculation criterion of the suture line is shown in formula (1).

$$E(x, y) = E_{color}^2(x, y) + E_{geometry}(x, y) \quad (1)$$

Among them, $E_{color}(x, y)$ represents the color difference evaluation value of the image, $E_{geometry}(x, y)$ represents the image structure difference evaluation value, and $E(x, y)$ is the overall difference evaluation value of the image. The calculation of E_{color} is shown in following.

$$E_{color} = \sqrt{(L_r - R_r)^2 + (L_g - R_g)^2 + (L_b - R_b)^2} \quad (2)$$

Among them, L and R are the overlapping parts of the two stitched images, and the subscript rgb represents the RGB layer respectively. The calculation of $E_{geometry}$ is shown in following.

$$E_{geometry}(x,y) = (S_x \times (I_L(x,y) - I_R(x,y)))^2 + (S_y \times (I_L(x,y) - I_R(x,y)))^2 \quad (3)$$

Among them, I represents the gray scale image, and S_x, S_y represents the Sobel operator, as shown in formulas (4) and (5).

$$S_x = \begin{bmatrix} -1 & 0 & 1 \\ -2 & 0 & 2 \\ -1 & 0 & 1 \end{bmatrix} \quad (4)$$

$$S_y = \begin{bmatrix} -1 & -2 & -1 \\ 0 & 0 & 0 \\ 1 & 2 & 1 \end{bmatrix} \quad (5)$$

Through formula (1), we can get the energy evaluation map E of the overlapping area. The smaller the $E(x,y)$, the smaller the difference in color and structure at that point. At the same time, the greater the $E(x,y)$, the greater the difference in color and structure of the point. The search for the best suture line is to find a path that divides the overlapping area into two parts, the left and right parts, and the sum \tilde{E} of the evaluation values of each point on the path is the smallest, as shown in formula (6). By finding the path with the smallest \tilde{E} , the local difference between the left and right images at the suture line is minimized, so that the stitching effect is the best.

$$\tilde{E} = \sum_{p \in line} E(p) \quad (6)$$

Among them, P is any point of the suture line, and m represents the overall difference evaluation value at point P. The best suture line found should make the \tilde{E} value the smallest.

The search strategy of the best suture line: each point in the first line of the evaluation graph is used as the starting point, and the nearest neighbor nodes in the five directions of left, left, bottom, bottom, right, and right are selected as candidate points, and the point with the smallest evaluation value among the candidate points is selected for each expansion, until it expands to the last row of the evaluation graph. Finally, from all the paths, the path with the smallest \tilde{E} is found as the best suture line. As shown in Figure 1, the subgraph (a) is the obtained evaluation graph, the subgraph (b) is the 5 expansion directions of any node, and the subgraphs (c)-(f) are the specific steps of point expansion.

Color texture mapping maps the two-dimensional pattern to the surface of the three-dimensional model by constructing the correspondence between the two-dimensional pattern and the three-dimensional surface, thereby constructing a very realistic virtual world, as shown in Figure 2. In Figure 2, (u,v) is a normalized texture coordinate, and its value range is a rectangular area defined from $(0,1)$ to $(1,1)$. The purpose of establishing color texture mapping is to find the corresponding relationship between (u,v) and (x,y,z) , and then assign the color at (u,v) in the texture pattern

to (x, y, z) in the three-dimensional surface to make the established three-dimensional model more realistic.

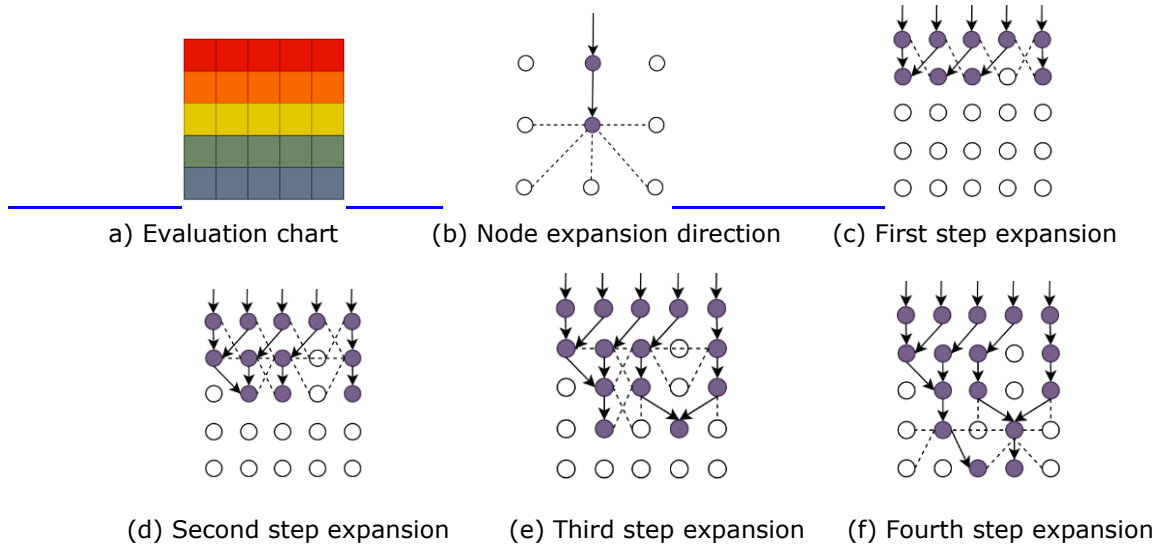


Figure 1: Search strategy of suture line.

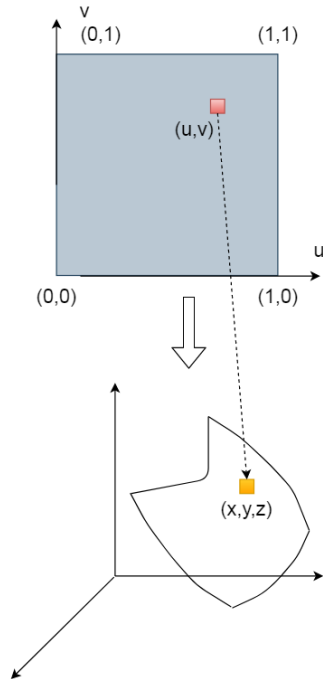


Figure 2: Texture mapping.

When designing 3D models, planes, spheres, cylinders and Nurbs surfaces are often used. For these space surfaces that can be represented by parameters, their parameters and texture coordinates are associated through a texture mapping algorithm to establish a corresponding relationship between (x, y, z) and (u, v) . Then, the texture pattern is mapped to the surface of the model, and the model is finally transformed from the scene space to the screen space to obtain a three-dimensional model covered with the texture pattern.

The calculation method of bump texture mapping is shown in formula (7).

$$P'(u, v) = P(u, v) + F(u, v)N(u, v) \quad (7)$$

Among them, $F(u, v)$ represents the uneven texture, $P(u, v)$ represents the function of the model surface before mapping, $N(u, v)$ represents the normal vector of the model surface, and $P'(u, v)$ is the new surface position obtained after calculation.

The normal vector at this point can be calculated by taking the vector product of the partial derivatives of $P'(u, v)$ in the u and v directions, as shown in the following formula.

$$N'(u, v) = N(u, v) + D(u, v) \quad (8)$$

$$D = F_u(N \times P_v) + F_v(N \times P_u) \quad (9)$$

Among them, D represents the disturbance vector, F_u, F_v represents the partial derivative of the uneven texture $F(u, v)$ with respect to u, v, and P_u, P_v represents the partial derivative of the model surface function $P(u, v)$ with respect to u, v. Therefore, as long as the partial derivative F_u, F_v of F is calculated, the normal vector N' after disturbance can be obtained. When the surface normal vector N line is appropriately perturbed, N' is obtained, and the texture pattern is shading and darkened accordingly, so that the originally smooth surface has a rough effect. Figure 3 is the effect comparison of color texture mapping and bump texture mapping.



(a) Color texture mapping



(b) Bump texture mapping

Figure 3: The effect of convex texture mapping.

Currently, the design of imitation digital camouflage mainly includes four steps: color space conversion, background main color extraction, determination of the unit size of the camouflage pattern, and generation of digital camouflage. The specific design process is shown in Figure 4.

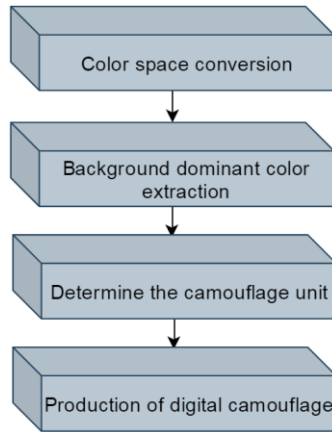


Figure 4: Design process of counterfeit digital camouflage.

In the three-dimensional world, three points are usually used to define a plane, and triangles are also one of the common facets in OpenGL. The normal line of a plane can be calculated from three points. We assume that there are three arbitrary points in the three-dimensional space, namely P_1 , P_2 , P_3 vector.

$$\begin{aligned} \vec{P_1P_2} &= P_2 - P_1 \\ \vec{P_2P_3} &= P_3 - P_2 \end{aligned} \quad (11)$$

As shown in Figure 5, the calculation of the normal vector n is shown in formula (12).

$$n = \frac{\vec{P_1P_2} \times \vec{P_2P_3}}{\left| \vec{P_1P_2} \times \vec{P_2P_3} \right|} \quad (12)$$

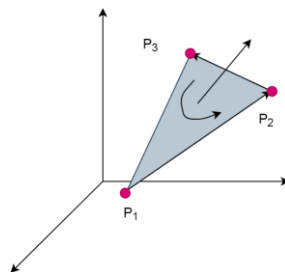


Figure 5: Calculation of normal vector.

For the surface of a three-dimensional target, its normal vector should point to the outside of the object. According to formula (12), it can be seen that the direction of the normal vector n is related

to the order of the cross product. If the positions of the two vectors are interchanged, n will point to the other direction. Therefore, it is necessary to specify the order of the vertices of the triangle, which can be clockwise or counterclockwise. Each triangle is composed of 3 vertices, and from the middle of the triangle, it can be seen that these 3 vertices set a winding order. Because the direction of n is related to the winding order of the vertices, OpenGL stipulates that the counterclockwise direction is the forward direction and the clockwise direction is the reverse direction, as shown in Figure 6.

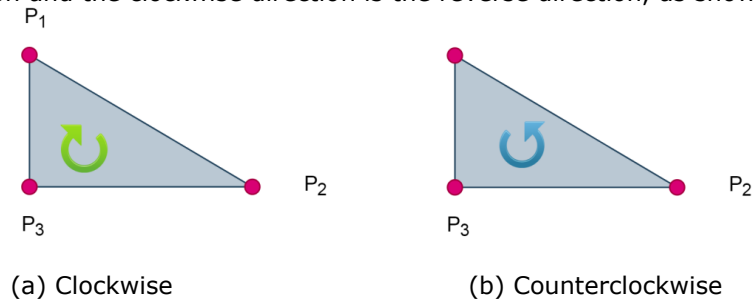


Figure 6: Vertex definition order.

The positive normal vector \hat{n} of the triangle patch is obtained by counterclockwise calculation, and the attribution of the surface element is determined based on this. This paper calculates the angle between the \hat{n} of the triangular facet and the normal vectors of the six planes of the cuboid to determine its attribution.

First, the 6 plane normal vectors of the cuboid are defined in the standard three-dimensional Cartesian coordinate system, as shown in formula (13), and the 6 plane normal vectors are shown in Figure 7.

$$\begin{cases} N_1 = (1, 0, 0) \\ N_2 = (-1, 0, 0) \\ N_3 = (0, 1, 0) \\ N_4 = (0, -1, 0) \\ N_5 = (0, 0, 1) \\ N_6 = (0, 0, -1) \end{cases} \quad (13)$$

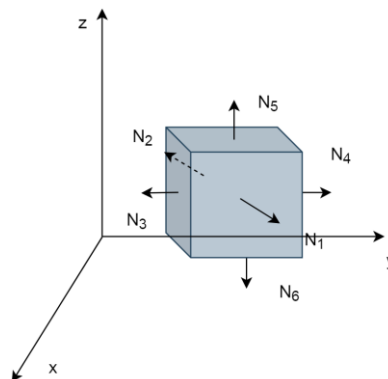


Figure 7: The plane normal vector of the interface.

The difference in orientation of the two patches can be characterized by the angle α of the normal vector of the patch, as shown in formula (14).

$$\cos \alpha = \frac{\hat{n} \cdot N}{|\hat{n}| |N|} \quad (14)$$

Since the included angle is $\alpha \in [0, \pi]$ and the cosine function is a monotonous decreasing function in the range of $[0, \pi]$, the larger $\cos \alpha$ means the smaller the normal vector angle between planes, and the smaller $\cos \alpha$ indicates the larger the normal vector angle between the planes. Therefore, this paper needs to calculate the cosine of the angle between the panel and the 6 planes, and find the intermediate plane with the largest value as the mapping plane of the panel.

In order to correspond to the two-dimensional texture pattern, the coordinates are usually set as a two-tuple (u, v) . At the same time, considering that the provided b texture patterns may have different sizes, (u, v) is standardized and limited to $[0, 1]$.

From another perspective, it can be considered that the mapping point on the intermediate interface is the forward projection of the target point on the intermediate interface, as shown in Figure 8.

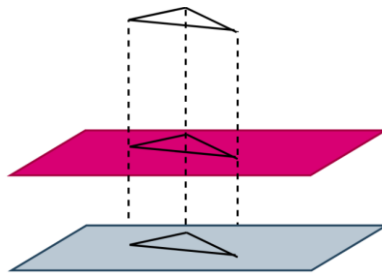


Figure 8: Schematic diagram of forward projection.

For any plane $Ax + By + Cz + D = 0$ in the three-dimensional space, the projection $P'(x_0, y_0, z_0)$ of any point $P(x, y, z)$ outside the plane on the plane can be calculated by formula (15).

$$\begin{cases} x_0 = x - At \\ y_0 = y - Bt \\ z_0 = z - Ct \end{cases} \quad (15)$$

Among them,

$$t = \frac{Ax + By + Cz + D}{A^2 + B^2 + C^2} \quad (16)$$

We use formula (15) to calculate the forward projection coordinate $P'(x, y, z)$ of each face element vertex on the plane to which it belongs, and then calculate their texture coordinate (u, v) according to the relative position of the projection point on each plane. For different intermediate planes, there

are certain differences in the calculation formulas. Here, the plane $x-D=0$ is taken as an example to analyze and the conversion formula (17) shows.

$$\begin{cases} u = \frac{Y - Y_{\min}}{Y_{\max} - Y_{\min}} \\ v = \frac{Z - Z_{\min}}{Z_{\max} - Z_{\min}} \end{cases} \quad (17)$$

Among them, Y_{\min} and Y_{\max} respectively are the minimum and maximum values of the plane on the Y-axis, and Z_{\min} and Z_{\max} are respectively the minimum and maximum values of the plane on the z-axis, as shown in Figure 9.

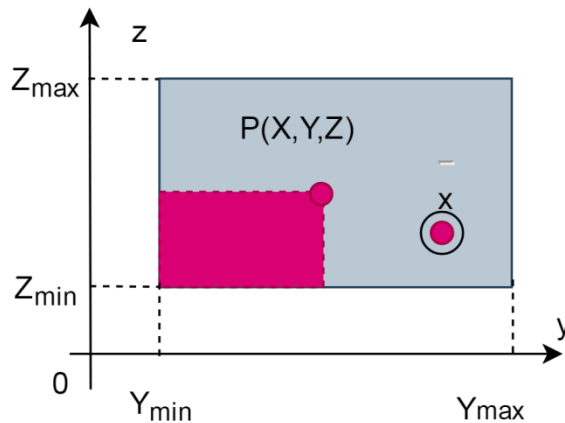


Figure 9: Schematic diagram of texture coordinate conversion.

Through formulas (15) and (17), the vertex coordinates of the three-dimensional target face element can be converted into texture coordinates. Because the texture coordinate is calculated with the lower left corner of the rectangle as the origin $(0,0)$, and the texture coordinate (u,v) represents the normalized coordinates of the point in the rectangle, the conversion formulas for the remaining five planes can be obtained by analogy with formula (17).

Formula (15) can be converted into matrix form, as shown in Equation (18).

$$P' = \begin{bmatrix} 1 - \frac{A^2}{A^2 + B^2 + C^2} & -\frac{AB}{A^2 + B^2 + C^2} & -\frac{AC}{A^2 + B^2 + C^2} \\ -\frac{AB}{A^2 + B^2 + C^2} & 1 - \frac{B^2}{A^2 + B^2 + C^2} & -\frac{BC}{A^2 + B^2 + C^2} \\ -\frac{AC}{A^2 + B^2 + C^2} & -\frac{BC}{A^2 + B^2 + C^2} & 1 - \frac{C^2}{A^2 + B^2 + C^2} \end{bmatrix} \quad (18)$$

$$\begin{bmatrix} x \\ y \\ z \end{bmatrix} = \frac{D}{A^2 + B^2 + C^2} \begin{bmatrix} A \\ B \\ C \end{bmatrix}$$

When $Q = (A, B, C)^T$, formula (18) can be simplified to formula (19). Among them, $\|Q\|_2$ represents the 2-norm of Q, and I is the identity matrix.

$$P' = \left(I - \frac{1}{\|Q\|_2^2} QQ^T \right) P - \frac{D}{\|Q\|_2^2} Q \quad (19)$$

For formula (17), the calculation of texture coordinate P_{uv} can be transformed into formula (20).

$$P_{uv} = \begin{bmatrix} 0 & \frac{1}{Y_{\max} - Y_{\min}} & 0 \\ 0 & 0 & \frac{1}{Z_{\max} - Z_{\min}} \end{bmatrix} \begin{bmatrix} x \\ y \\ z \end{bmatrix} - \begin{bmatrix} \frac{Y_{\min}}{Y_{\max} - Y_{\min}} \\ \frac{Z_{\min}}{Z_{\max} - Z_{\min}} \end{bmatrix} \quad (20)$$

The texture coordinate conversion method of each intermediate plane is similar, so the conversion matrix of the other planes can be obtained by analogous formulas (17) and (20).

4 CONSTRUCTION PROCESS SIMULATION OF BUILDING DECORATION BASED ON BIM AND COMPUTER-AIDED TECHNOLOGY

This article combines BIM and computer-aided technology to simulate the construction process of building decoration. Moreover, this paper uses BIM software to establish a basic application platform with BIM model as the core idea, and uses modeling software, BIM review, BIM viewer, etc. to apply the model to realize the horizontal integrated application of technology, production and owners. In addition, this paper simulates the construction process by integrating key information such as design, pre-settlement, materials, and construction teams through the BIM model, as shown in Figure 10.



Figure 10: Construction process simulation of building decoration based on BIM and computer-aided technology.

On the basis of the above analysis, the construction process of building decoration is simulated. First, this paper combines BIM and computer-aided technology to evaluate the design of architectural decoration, and design 80 groups of architectural decorations for a residential building, and score them through some architectural decoration design experts. The results are shown in Table 1 and Figure 11.

Number	Scores	Number	Scores	Number	Scores	Number	Scores
1	94.2	21	89.6	41	88.6	61	90.4
2	94.3	22	87.7	42	87.0	62	83.8
3	91.2	23	85.8	43	91.6	63	92.0
4	81.4	24	88.9	44	83.0	64	82.1
5	87.3	25	91.2	45	89.9	65	82.2
6	89.4	26	86.8	46	88.9	66	86.7
7	83.5	27	87.9	47	86.4	67	87.5
8	88.3	28	90.8	48	92.1	68	83.6
9	83.7	29	81.7	49	81.7	69	89.5
10	94.3	30	82.0	50	85.6	70	93.6
11	93.4	31	84.5	51	85.9	71	82.3
12	90.1	32	82.7	52	85.2	72	90.9
13	94.1	33	88.5	53	84.5	73	84.4
14	88.7	34	87.3	54	89.2	74	89.7
15	84.5	35	93.9	55	83.4	75	86.7
16	82.9	36	87.7	56	90.9	76	88.7
17	84.5	37	88.8	57	94.6	77	90.7
18	83.6	38	86.7	58	89.6	78	86.5
19	83.5	39	88.0	59	87.4	79	90.2
20	91.9	40	90.2	60	81.4	80	85.9

Table 1: Statistical table of the scores of architectural decoration design.

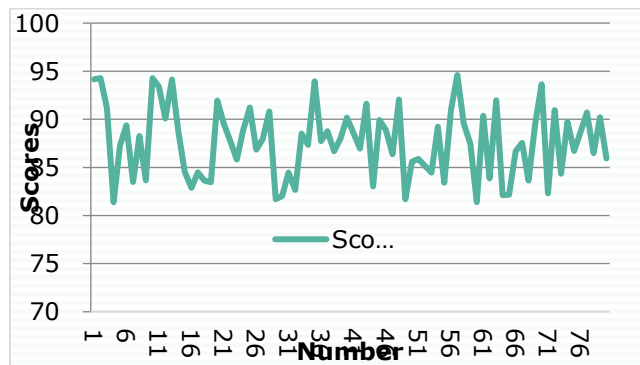


Figure 11: Statistical diagram of the scores of architectural decoration design.

It can be seen from the above chart that the combination of BIM and computer-aided technology can effectively improve the design effect of architectural decoration in architectural decoration design and achieve better user satisfaction. Next, this paper simulates the construction process of building decoration and calculates its suitability degree with actual construction. The results are shown in Table 2 and Figure 12.

Number	suitability	Number	suitability	Number	suitability	Number	suitability
1	0.766	21	0.678	41	0.648	61	0.722
2	0.768	22	0.745	42	0.679	62	0.811
3	0.671	23	0.732	43	0.747	63	0.745
4	0.749	24	0.746	44	0.673	64	0.769
5	0.732	25	0.711	45	0.646	65	0.631
6	0.761	26	0.788	46	0.686	66	0.762
7	0.682	27	0.677	47	0.667	67	0.659
8	0.693	28	0.737	48	0.756	68	0.743
9	0.635	29	0.753	49	0.728	69	0.664
10	0.655	30	0.700	50	0.757	70	0.806
11	0.777	31	0.792	51	0.693	71	0.727
12	0.633	32	0.639	52	0.713	72	0.691
13	0.751	33	0.636	53	0.698	73	0.718
14	0.806	34	0.752	54	0.671	74	0.750
15	0.654	35	0.664	55	0.728	75	0.785
16	0.720	36	0.687	56	0.744	76	0.806
17	0.660	37	0.721	57	0.797	77	0.758
18	0.740	38	0.779	58	0.631	78	0.780
19	0.778	39	0.743	59	0.662	79	0.689
20	0.658	40	0.682	60	0.743	80	0.776

Table 2: Statistical table of the matching degree of the construction process simulation of building decoration.

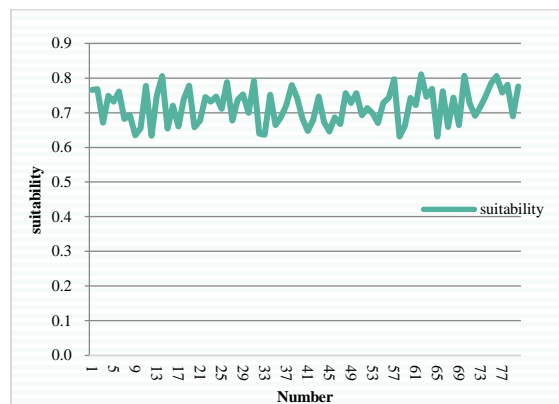


Figure 12: Statistical diagram of the suitability degree of the construction process simulation of building decoration.

From the above analysis results, the model constructed in this paper can play an important role in the simulation process of building decoration construction, and can provide reference for subsequent construction, and expose some possible problems in advance, so it has a good construction reference significance.

5 CONCLUSION

The integration of informatization and simulation in the building decoration industry will place the construction industry in a huge wave of change. As an important technical means to integrate the two, BIM model technology has now set off a revolutionary chapter in the construction industry. At present, BIM model technology has achieved certain development, and the formed application system is also relatively mature. When it is applied to the design and construction links, there is good continuity, and the model technology results can be applied in the operation and maintenance stage. Aiming at the content of building decoration engineering design and construction process, this paper proposes a decoration work process based on BIM visualization and collaborative model technology. This process is more beneficial to the application of BIM technology and can improve the work efficiency of building decoration engineering. In addition, this paper combines BIM technology and computer-aided technology to simulate the construction process of building decoration, and verifies the effect through experiments. The research results show that the effect of the method proposed in this paper is very significant.

Yugang Dong, <https://orcid.org/0009-0002-3421-1335>

Yingqun Zhang, <https://orcid.org/0009-0007-0218-1545>

Fangfang Sang, <https://orcid.org/0009-0001-3302-6173>

ACKNOWLEDGEMENT

Science and Technology Development Plan Project Of Weifang 2020GX089.

REFERENCES

- [1] Brock Glasgo, A.; Chris Hendrickson, B.; Inês Lima Azevedo, a.: Assessing the value of information in residential building simulation: Comparing simulated and actual building loads at the circuit level, *Applied Energy*, 203(10), 2017, 348-363. <https://doi.org/10.1016/j.apenergy.2017.05.164>
- [2] Andriamamonjy, A.; Saelens, D.; Klein, R.: An automated IFC-based workflow for building energy performance simulation with Modelica, *Automation in Construction*, 91, 2018, 166-181. <https://doi.org/10.1016/j.autcon.2018.03.019>
- [3] Blocken, B.: LES over RANS in building simulation for outdoor and indoor applications: A foregone conclusion?, *Building Simulation*, 11(2), 2018, 1-50. <https://doi.org/10.1007/s12273-018-0459-3>
- [4] Boukhris, Y.; Gharbi, L.; Ghrab-Morcos, N.: Coupling the building simulation tool ZAER with a sunspot model. Case study in Tunis, *Energy & Buildings*, 70, 2014, 1-14. <https://doi.org/10.1016/j.enbuild.2013.11.002>
- [5] Brouns, J.; Nassiopoulos, A.; Bourquin, F.; et al.: Dynamic building performance assessment using calibrated simulation, *Energy & Buildings*, 122(jun.), 2016, 160-174. <https://doi.org/10.1016/j.enbuild.2016.04.015>
- [6] Lee, B. H.; Yee, S. W.; Kang, D. H.; et al.: Multi-zone simulation of outdoor particle penetration and transport in a multi-story building, *Building Simulation*, 10(4), 2017, 525-534. <https://doi.org/10.1007/s12273-016-0340-1>

- [7] Chen, H.; Li, Z.; Wang, X.; et al.: A graph- and feature-based building space recognition algorithm for performance simulation in the early design stage, *Building Simulation*, 11(2), 2017, 1-12. <https://doi.org/10.1007/s12273-017-0412-x>
- [8] Cornaro, C.; Sapori, D.; Bucci, F.; et al.: Thermal performance analysis of an emergency shelter using dynamic building simulation, *Energy & Buildings*, 88(feb.), 2015, 122-134. <https://doi.org/10.1016/j.enbuild.2014.11.055>
- [9] Eguia Oiler, P.; Alonso Rodriguez, J. M.; Saavedra Gonzalez, A.; et al.: Improving the calibration of building simulation with interpolated weather datasets, *Renewable Energy*, 122, 2018, 608-618. <https://doi.org/10.1016/j.renene.2018.01.100>
- [10] Garay Martinez, R.; Riverola, A.; Chemisana, D.: Disaggregation process for dynamic multidimensional heat flux in building simulation, *Energy & Buildings*, 148(aug.), 2017, 298-310. <https://doi.org/10.1016/j.enbuild.2017.05.029>
- [11] Gasparin, S.; Berger, J.; Dutykh, D.; et al.: An improved explicit scheme for whole-building hygrothermal simulation, *Building Simulation*, 11(003), 2018, 465-481. <https://doi.org/10.1007/s12273-017-0419-3>
- [12] Hong, T.; Chen, Y.; Belafi, Z.; et al.: Occupant behavior models: A critical review of implementation and representation approaches in building performance simulation programs, *Building Simulation*, 11(001), 2017, 1-14. <https://doi.org/10.1007/s12273-017-0396-6>
- [13] Hong, T.; Chou, S. K.; Bong, T. Y.: Building simulation: an overview of developments and informations, *Building & Environment*, 35(4), 2014, 347-361. [https://doi.org/10.1016/S0360-1323\(99\)00023-2](https://doi.org/10.1016/S0360-1323(99)00023-2)
- [14] Mantesi, E.; Hopfe, C. J.; Cook, M. J.; et al.: The modelling gap: Quantifying the discrepancy in the representation of thermal mass in building simulation, *Building and Environment*, 131(mar.), 2018, 74-98. <https://doi.org/10.1016/j.buildenv.2017.12.017>
- [15] Pengyuan, S.; William, B.; Yunky, Y.: Development of a lightweight building simulation tool using simplified zone thermal coupling for fast parametric study, *Applied Energy*, 223(aug.1), 2018, 188-214. <https://doi.org/10.1016/j.apenergy.2018.04.039>
- [16] Ren, Z.; Wang, X.; Chen, D.; et al.: Constructing weather data for building simulation considering urban heat island, *Building Service Engineering*, 35(1), 2014, 69-82. <https://doi.org/10.1177/0143624412467194>
- [17] Shiel, P.; Tarantino, S.; Fischer, M.: Parametric Analysis of Design Stage Building Energy Performance Simulation Models, *Energy and Buildings*, 172(aug.), 2018, 78-93. <https://doi.org/10.1016/j.enbuild.2018.04.045>
- [18] Verbruggen, B.; Driesen, J.: Grid impact indicators for active building simulation, *IEEE Transactions on Sustainable Energy*, 6(1), 2017, 43-50. <https://doi.org/10.1109/TSTE.2014.2357475>
- [19] Wang, H.; Zhai, Z.: Advances in Building Simulation and Computational Techniques: A Review between 1987 and 2014, *Energy & Buildings*, 128(sep.), 2016, 319-335. <https://doi.org/10.1016/j.enbuild.2016.06.080>
- [20] Wang, M.; Wright, J.; Brownlee, A.; et al.: A comparison of approaches to stepwise regression on variables sensitivities in building simulation and analysis, *Energy & Buildings*, 127(sep.), 2016, 313-326. <https://doi.org/10.1016/j.enbuild.2016.05.065>
- [21] Zermani, M. A.; Feki, E.; Mami, A.: Building simulation model of infant-incubator system with decoupling predictive controller, *Irbm*, 35(4), 2014, 189-201. <https://doi.org/10.1016/j.irbm.2014.07.001>
- [22] Zhai, Z. J.; McNeill, J. S.: Roles of building simulation tools in sustainable building design, *Building Simulation*, 7(2), 2014, 107-109. <https://doi.org/10.1007/s12273-013-0169-9>
- [23] Zhua, M.; Pan, Y.; Huang, Z.; et al.: An alternative method to predict future weather data for building energy demand simulation under global climate change, *Energy and Buildings*, 113(Feb.), 2016, 74-86. <https://doi.org/10.1016/j.enbuild.2015.12.020>